Journal of Biomolecular NMR, **11:** 119–133, 1998.
KLUWER/ESCOM
© 1998 *Kluwer Academic Publishers. Printed in Belgium.*

Detailed NMR analysis of the heme–protein interactions in component IV *Glycera dibranchiata* monomeric hemoglobin-CO

Steve L. Alam[a], Brian F. Volkman[b], John L. Markley[b] and James D. Satterlee[a,*]
[a]*Department of Chemistry, Washington State University, Pullman, WA 99164-4630, U.S.A.* [b]*National Magnetic Resonance Facility at Madison, Department of Biochemistry, University of Wisconsin-Madison, 420 Henry Mall, Madison, WI 53706, U.S.A.*

Received 6 August 1997; Accepted 10 September 1997

Key words: complete assignments, heme, heme protein, secondary structure

Abstract

Complete ^{13}C, ^{15}N, and ^{1}H resonance assignments have been obtained for the recombinant, ferrous CO-ligated form of component IV monomeric hemoglobin from *Glycera dibranchiata*. This 15642 Da myoglobin-like protein contains a large number of glycine and alanine residues (47) and a heme prosthetic group. Coupling constant information has allowed the determination of χ^1 and χ^2 torsion angles, backbone ϕ angles, as well as 43 of 81 possible assignments to $H^{\beta 2/\beta 3}$ pairs. The $^{13}C^{\alpha}$, $^{13}C^{\beta}$, $^{13}C'$, and $^{1}H^{\alpha}$ assignments yield a consensus chemical shift index (CSI) that, in combination with NOE information and backbone torsion angles, defines seven distinct helical regions for the protein's global architecture. Discrepancies between the CSI and NOE/$^{3}J_{HNH\alpha}$-based secondary structure definitions have been attributed to heme ring current shifts on the basis of calculations from a model structure [Alam et al. (1994) *J. Protein Chem.*, **13**, 151–164]. The agreement can be improved by correcting the $^{1}H^{\alpha}$ chemical shifts for the ring current contributions. Because the holoprotein was assembled from isotopically enriched globin and natural isotope-abundance heme, data from ^{13}C-filtered/^{13}C-edited and ^{13}C-filtered/^{13}C-filtered 2D NOESY experiments could be used to determine complete heme proton assignments and to position the heme within the protein. The results confirm the unusual presence of Phe^{31}(B10) and Leu^{58}(E7) side chains near the heme ligand binding site which may alter the polarity and steric environment and thus the functional properties of this protein.

Abbreviations: GMH4, component IV *Glycera dibranchiata* monomeric hemoglobin; GMH4CO, CO-ligated form of component IV *Glycera dibranchiata* monomeric hemoglobin; Hb, hemoglobin; Mb, myoglobin; GMH, *Glycera dibranchiata* monomeric hemoglobin; HSQC, heteronuclear single quantum coherence; HMBC, heteronuclear multiple-bond correlation; SE, sensitivity enhancement; INEPT, insensitive nuclear enhancement by polarization transfer; TOCSY, total correlation spectroscopy; NOESY, nuclear Overhauser effect spectroscopy.

Introduction

The ground rules for the mechanism by which hemoglobin (Hb) and myoglobin (Mb) control ligand affinity at the heme prosthetic group have been established from detailed comparisons of structures of ligated and unligated forms of these proteins (Baldwin and Chothia, 1979; Shaanan, 1983; Perutz et al., 1987; Quillin et al., 1993). Several possible ligand trajectories that involve the movement of flexible regions within the protein have been proposed on the basis of molecular dynamics simulations (Case and Karplus, 1979; Kottalam and Case, 1988). Recent time-resolved X-ray crystallography of photolyzed Mb-CO provides structural snapshots of the amino acid and heme reorganizations that are important in CO recombination and rebinding (Srajer et al., 1996). Amino acids that play a role in these proposed mech-

* To whom correspondence should be addressed.

anisms (B10, CD3, CD4, E10, E11, and the highly conserved E7 distal histidine) are, for the most part, localized to the distal side of the heme, although proximal residues and surface amino acids have been shown to influence ligand kinetics in Mb (Olson et al., 1988; Lambright et al., 1989; Egeberg et al., 1990; Rohlfs et al., 1990; Carver et al., 1991, 1992; Ideka-Saito et al., 1991; Petric et al., 1991; Smerdon et al., 1991; Adachi et al., 1992; Gibson et al., 1992).

Interest in the *Glycera dibranchiata* monomeric hemoglobin (GMH) proteins arose from early kinetic studies that disclosed unique binding properties of these proteins and the discovery of the naturally occurring E7-His to Leu substitution in all of the monomeric Hbs of this marine annelid. One of the three major monomeric Hbs from *Glycera dibranchiata* displayed significantly lower affinities for CN^- and O_2, and a much higher affinity for CO, when compared to Mb (Parkhurst et al., 1980; Rohlfs et al., 1990). Both the association and dissociation rate constants for O_2 and CO are significantly higher for this monomeric Hb than for Mb. The cyanide association rate constants observed for the ferric forms of all three major monomeric Hbs are up to 5 orders of magnitude slower than for other heme proteins (Mintorovitch and Satterlee, 1988; Mintorovitch et al., 1989). The naturally occurring E7 leucine found in all GMHs may account for the altered ligand binding properties of these proteins (Parkhurst et al., 1980; Mintorovitch and Satterlee, 1988; Mintorovitch et al., 1989). Thus, comparisons of GMHs with other Mbs and Hbs provide the opportunity of studying the structural and dynamic roles of the distal pocket residues.

A puzzling factor with investigations of GMHs by different laboratories has been a heterogeneity in the reported physical properties of these proteins. Recent studies (Green et al., 1997; Teske et al., 1997) suggest that the GMH fraction contains more extensive heterogeneity than previously realized, with as many as 10 individual monomeric Hbs (among these are the three major monomeric proteins GMH2, GMH3, and GMH4). Different laboratories studying the effects of the naturally occurring E7 leucine substitution in GMHs likely have used protein mixtures or differing isoforms. This may account for the variability in reported results. An example of the confusion in protein identity comes from two refined X-ray structures of a GMH (Arents and Love, 1989; Braden et al., 1994). The M_r of the crystallized protein (as calculated from the primary sequence) does not correspond to any of the M_r values for GMHs determined by mass spectrometry (Green et al., 1997). In addition, its primary sequence does not agree with sequences of the three major monomeric Hbs (Alam et al., 1994b; Teske et al., 1997).

Despite this confusion, key features of the monomeric Hbs have been identified. NMR data (Cooke and Wright, 1985a, 1987; Cooke et al., 1987) and protein sequencing results (Alam et al., 1994b; Teske et al., 1997) confirm the distal E7-Leu in GMH2–4, and place a phenylalanine at position B10 in one of the three major monomeric Hbs (GMH4 in our laboratory). From these details and the aforementioned crystal structure, we constructed a model of the GMH4 protein which displays an unusually apolar heme pocket.

The Satterlee laboratory has been studying isolated preparations of the three major monomeric Hbs in order to establish a reliable database upon which further mechanistic interpretations of these Hbs can be made (Kandler and Satterlee, 1983; Kandler et al., 1984; Cross and Wright, 1985; Mintorovitch and Satterlee, 1988; Mintorovitch et al., 1989; Alam et al., 1994a,b; Braden et al., 1994). Detailed descriptions of the structural and dynamic features of these proteins are needed in order to understand the anomalous ligation properties of the GMHs. It will be of interest to compare these results with similar results for myoglobin and myoglobin mutants that have been designed to mimic the Hbs of *G. dibranchiata* (Quillin et al., 1993). This study represents the first detailed structural analysis of a well-characterized GMH.

Presented here are the complete ^{13}C, ^{15}N, and ^1H resonance assignments for the CO-ligated form of component IV *Glycera dibranchiata* monomeric hemoglobin (GMH4CO), determined from a set of standard multi-dimensional triple-resonance experiments. The ferrous CO-ligated form of this protein was chosen for this study because it is diamagnetic and carbon monoxide is a physiologically significant heme ligand. The large number of glycine and alanine residues, as well as the helical nature of this protein, presented challenges to the assignment process, but these were surmounted with the use of modern triple-resonance NMR experiments. Stereospecific assignments for 43 of the 81 pairs of prochiral H^β protons, all of the valine H^γ methyls, and 5 of the 10 leucine H^δ methyls have been completed. Complete ^1H assignments for the heme prosthetic group, including both of its propionic acid side chains, were obtained through analysis of ^1H NMR data. Assignments of the heme

resonances as well as NOEs involving the heme made use of $^{13}C/^{15}N$-filtered experiments.

The results of these NMR studies are in agreement with a previously proposed model for the heme active site of component IV *Glycera dibranchiata* monomeric hemoglobin (GMH4) (Alam et al., 1994b). The current results place LeuE7, PheB10, and 17 other amino acids within the heme pocket in agreement with the model structure and previous NMR data (Cooke et al., 1987). Seven helical regions and five linker regions were defined by the following experimental evidence: (i) the chemical shift index (CSI) of the $^{13}C^{\alpha}$, $^{13}C^{\beta}$, $^{13}C'$, and $^{1}H^{\alpha}$ resonances; (ii) structurally defining sequential NOEs; (iii) $^{3}J_{HNH\alpha}$ scalar coupling constants; and (iv) distinctive helix-capping NOEs. For several residues, the (CSI) secondary structure definition was found to conflict with the NOE and backbone dihedral angle information; this is attributed to the influence of ring current effects from the heme cofactor on the observed chemical shift. This work sets the foundation for a complete structural and dynamic analysis of GMH4.

Materials and methods

Sample preparation

GMH4 was expressed as the apoprotein (GMG4) in *Escherichia coli* as previously described (Alam et al., 1994a), with the exception that the cDNA encoding GMG4 was sub-cloned into the pET9D expression vector (Novagen, Madison, WI) to confer kanamycin resistance. To produce isotopically labeled protein samples, this strain was grown and induced in minimal media (M9) with glucose and NH_4Cl as the sole carbon and nitrogen sources, respectively.

For ^{15}N labeling, the M9 medium contained 0.8% glucose, 0.2% $^{15}NH_4Cl$ (99% enriched, Isotec, Miamisburg, OH), 100 μg/ml kanamycin, 10 ml/l of a vitamin mixture (10 mg/100 ml each of biotin, choline-chloride, folic acid, niacinamide, D-pantothenate, pyridoxal, and 1 mg/100 ml of riboflavin (Venters et al., 1991)), and the M9 salts (6% Na_2HPO_4, 3% KH_2PO_4, 0.5% NaCl, 2 mM $MgSO_4$, and 0.1 mM $CaCl_2$ (Maniatis et al., 1986)). The same medium was used for the $^{13}C/^{15}N$ labeling except for the substitution of 0.2% [99% ^{13}C]-glucose (Isotec). The large-scale cultures (3 × 1 l) were initiated by diluting the inoculum 1:100 into fresh medium. The cultures were incubated at 34 °C with aeration until OD_{600} reached 0.3, at which time the cultures were cooled to 21 °C and isopropyl-β-D-thiogalactopyranoside (IPTG) was added to a final concentration of 1 mM to induce protein expression. Following induction, the cultures were incubated at 21 °C for 12 h and then harvested. The protein was constituted with b-type hemin-Cl (Porphyrin Products, Ogden, UT) and purified in the oxidized (Fe^{3+}) form as described previously (Alam et al., 1994a). Typically, yields gave 16–20 mg of purified holoprotein per liter of culture. The absence of an N-terminal methionine in the expressed protein was confirmed by mass spectrometry.

Purified ferric GMH4 was reduced by adding a 50% molar excess of sodium dithionite, buffered to pH 6.8 in $CO_{(g)}$-saturated 100 mM potassium phosphate buffer (pH 6.80). The excess sodium dithionite was removed with several washes of buffer in an ultrafiltration cell (Amicon, Beverly, MA) as the sample was being exchanged into the CO-saturated NMR buffer (100 mM potassium phosphate, 100 mM KCl, pH 5.0, 10% D_2O). The samples were transferred to NMR tubes, after being filtered through a 0.2 μm filter, topped with $CO_{(g)}$, and sealed. Final protein concentrations were 3.5 and 3 mM for the ^{15}N- and $^{13}C/^{15}N$-labeled samples, respectively. All experiments discussed below were performed on samples containing 100 mM potassium phosphate, 100 mM KCl, pH 5.0, in 90% H_2O/10% D_2O.

NMR data collection

All spectra were recorded at 20 °C on Bruker DMX500 and DMX600 spectrometers equipped with triple-resonance $^{1}H/^{13}C/^{15}N$ probes and triple-axis pulsed field gradient capabilities. Quadrature detection in the indirectly detected dimensions was obtained by the States-TPPI method (Marion and Wüthrich, 1983). All spectra collected on Bruker instruments at the National Magnetic Resonance Facility at Madison (NMRFAM) (University of Wisconsin-Madison) made use of digital filtering capabilities.

The assignments and description of secondary structure presented here were based on the following set of experiments: 2D $^{1}H/^{15}N$ SE-HSQC (Zhang et al., 1994), SE-HNCO (Grzesiek and Bax, 1992; Muhandiram and Kay, 1994), SE-HNCA (Grzesiek and Bax, 1992; Kay et al., 1994; Muhandiram and Kay, 1994), SE-HN(CO)CA (Grzesiek and Bax, 1992; Kay et al., 1994), SE-HNCACB (McCoy and Mueller, 1992; Wittekind and Mueller, 1993; Muhandiram and Kay, 1994), SE-CBCA(CO)NH (Grzesiek and Bax, 1992; Kay et al., 1994), SE-HCACO (Powers et al., 1990; Bazzo et al., 1995), SE-C(CO)NH C-TOCSY

(Grzesiek et al., 1993a), 3D SE-^{15}N-edited and ^{13}C-edited NOESY, 3D ^{15}N-edited TOCSY, 2D CT-^{13}C/^{1}H HSQC (Santoro and King, 1992), 3D HCCH-TOCSY (Kay et al., 1993) and SE-HBHA(CBCACO)NH (Grzesiek and Bax, 1992, 1993; Muhandiram and Kay, 1994). All experiments that included a ^{1}H/^{15}N INEPT at the beginning and a ^{15}N/^{1}H INEPT sequence as the final transfer before signal observation included sensitivity enhancement (SE) with gradient coherence selection, and most included a water flip-back pulse scheme to keep water as close to equilibrium as possible and reduce amide intensity loss due to saturation transfer (Kay et al., 1994). Gradient pulses as a combination of X- and Z-gradients at the 'magic angle' (Warren et al., 1993; van Zijl et al., 1995) were used for coherence selection in a number of experiments to maximize water suppression. Experimental details of each experiment, including transmitter offsets, sweep widths and complex points for each dimension, as well as mixing times and final processed matrix sizes, are given in Table 1.

Since the heme-b used during constitution to form the holoprotein was not isotopically enriched, isotope edited and filtered experiments were used to select either heme or non-heme resonances in a defined dimension of a NOESY experiment. Specifically, an F1-^{13}C-edited/F2-^{13}C-filtered 2D ^{1}H/^{1}H NOESY spectrum (Lee et al., 1994) was used to identify all NOEs that originated from ^{13}C-attached protons in F1 and whose destination was ^{12}C-bound protons of the heme in F2. In addition a 2D ^{1}H/^{1}H NOESY with ^{13}C filtering in both the F1 and F2 dimensions (Ikura and Bax, 1992) was used to identify intra-heme NOEs. In both cases, pulse sequences were implemented as previously described, but with the addition of gradients for artifact suppression and WATERGATE water suppression (Piotto et al., 1992).

Quantitative *J*-correlation experiments were used for stereoassignments and qualitative determination of torsion angles. The 3D HNHB (Archer et al., 1991), HN(CO)HB (Grzesiek et al., 1992), and ^{15}N-edited TOCSY and NOESY experiments were used for stereospecific assignment of methylene H$^{\beta}$ protons and χ^1 rotamer determination. Stereospecific assignments of prochiral valine H$^{\gamma}$ methyls and determinations of χ^1 torsion angles for valine, threonine and isoleucine residues were accomplished with data from the 2D J_{NC} (Vuister et al., 1993), and J_{CC} (Grzesiek et al., 1993b) spin-echo difference experiments. H$^{\delta}$ methyl stereoassignments and χ^2 torsion angles for some leucine residues were obtained from analysis of long-range carbon-carbon couplings (LRCC) (Bax et al., 1992) and intraresidue NOE intensities. The 3D HNHA experiment (Vuister and Bax, 1993; Kuboniwa et al., 1994) was used to obtain $^{3}J_{HNH\alpha}$ values and to determine qualitative backbone ϕ angles.

Data analysis

All experiments were processed with either FELIX95 or FELIX 2.30 software (MSI, San Diego, CA) with user written macros. In most cases, the indirect dimension with the least amount of digitization was extended with linear prediction by no more than 50% of the original data size. The initial incremented delays for the indirect experiments were set in a manner that allowed predictable phasing in each dimension, which in some instances required linear prediction of a new first point prior to Fourier transformation (Edison et al., 1994). Finally, a window function of either a skewed-shifted sinebell-squared or a shifted sinebell was applied to each FID prior to zero filling to the final dimensions (as outlined in Table 1). The resulting data sets were Fourier transformed and phase corrected.

All ^{1}H dimensions were referenced indirectly to a separate 10 mM DSS (2,2-dimethyl-2-silapentane-5-sulfonate) sample at 20 °C in the NMR buffer discussed above. ^{13}C and ^{15}N dimensions were referenced indirectly to DSS as previously described (Wishart et al., 1995b). Chemical shifts for all cross peaks were tabulated by the PPFLX peak-picking software (http://www.nmrfam.wisc.edu/roger/Software/peakpick/pp_main.html). Referenced outputs from PPFLX for each experiment could be compiled into separate databases to be searched for assignment information in a semi-automated manner. This was accomplished using PERL (Wall and Schwartz, 1991) scripts written to provide correlations from each type of experiment, and to tabulate an assignment database. This approach expedited the assignment process and quickly identified regions where assignments would be difficult. This same script approach was used to search the database of assignments in order to interpret the NOEs in the ^{13}C-edited and ^{15}N-edited 3D NOESYs that were used for defining secondary structural elements.

The CSI was calculated for each assigned $^{13}C^{\alpha}$, $^{13}C^{\beta}$, $^{13}C'$ and $^{1}H^{\alpha}$ resonance as previously described (Wishart et al., 1992, 1995a; Wishart and Sykes, 1994). For glycine residues with non-degenerate $^{1}H^{\alpha}$ chemical shifts, the average was used in calculating the $^{1}H^{\alpha}$ CSI. To evaluate effects of ring current shifts on CSI values, ring current shifts estimated (by pre-

Table 1. Parameters for NMR experiments used in the $^{1}H/^{13}C/^{15}N$ assignments of GMH4CO

Experiment	^{1}H		D2			D3			Matrix dimensions[c]	Mixing[d]
	SF (MHz)[a]	SW (Hz)	Nucleus	SW (Hz)	N*[b]	Nucleus	SW (Hz)	N*		
HNCO[e]	500.13	7716.05	$^{13}C'$	1666.67	160	^{15}N	1666.67	40	512 × 256 × 128	
HCACO[e]	500.13	7716.05	$^{13}C^{\alpha}$	3571.43	27	$^{13}C'$	1666.67	96	512 × 256 × 128	
HNCA[e]	500.13	7716.05	$^{13}C^{\alpha}$	3571.43	96	^{15}N	1666.67	40	512 × 256 × 128	
HN(CO)CA[e]	500.13	7716.05	$^{13}C^{\alpha}$	3571.43	56	^{15}N	1666.67	40	512 × 256 × 128	
CBCA(CO)NH[e]	500.13	7716.05	$^{13}C^{\alpha\beta}$	7692.3	44	^{15}N	1666.67	40	512 × 256 × 128	
HNCACB[e]	500.13	7716.05	$^{13}C^{\alpha\beta}$	7692.3	80	^{15}N	1666.67	40	512 × 256 × 128	
C(CO)NH[e,g]	499.84	7716.05	^{13}C	8333.47	64	^{15}N	1666.67	40	512 × 256 × 128	
HBHA(CO)NH[e]	499.84	7716.05	^{1}H	4149.4	53	^{15}N	1666.67	40	512 × 256 × 128	
HCCH-TOCSY[e,g]	500.13	4006.40	^{1}H	4006.4	128	^{13}C	4000	64	512 × 256 × 128	18.9
^{15}N-TOCSY[e]	500.13	7692.30	^{1}H	7692.30	150	^{15}N	1666.67	36	512 × 512 × 128	51.7
^{15}N-NOESY[e]	500.13	7716.05	^{1}H	7716.05	128	^{15}N	1666.67	32	512 × 512 × 128	100
$^{15}N/^{1}H$ HSQC	500.13	7716.05	^{15}N	1666.67	512				1024 × 1024	
CT-HSQC ^{13}C	500.13	4006.40	^{13}C	4000	114				1024 × 512	
J_{NC}[f]	600.13	10000	^{13}C	5000	256				512 × 512	
J_{CC}[f]	600.13	10000	^{13}C	5000	256				512 × 512	
LRCC[f]	600.13	10000	^{13}C	5000	128				512 × 512	
HNHA[f]	600.13	8333.33	^{1}H	8333.33	80	^{15}N	2000	50	512 × 512 × 64	
HNHB[f]	600.13	8333.33	^{1}H	8333.33	150	^{15}N	2000	50	512 × 512 × 64	
HN(CO)HB[f]	600.13	8333.33	^{1}H	6944.44	75	^{15}N	2000	40	512 × 256 × 64	
^{13}C-NOESY[f,g]	600.13	8333.33	^{1}H	9090.91	256	^{13}C	6250	48	512 × 512 × 128	80
^{13}C-NOESY[h]	499.84	6944.44	^{1}H	10000	128	^{13}C	2500	32	512 × 512 × 64	80
$^{13}C/^{12}C$-NOESY[i]	600.13	10000	^{1}H	7812.5	128				1024 × 1024	100
$^{12}C/^{12}C$-NOESY[j]	600.13	8333.33	^{1}H	8333.33	512				1024 × 1024	125

[a] Spectral frequency used for this experiment. 499.84, 500.13 and 600.13 denote the DMX500i, DMX500ii and DMX600 instruments, respectively, housed at NMRFAM (University of Wisconsin).
[b] Number of complex points collected in this indirect dimension.
[c] Final processed matrix size.
[d] Time in ms for NOESY or isotropic mixing times.
[e] Experiments used for backbone assignments.
[f] For stereospecific assignments and dihedral calculation.
[g] To complete side-chain assignments.
[h] 3D ^{13}C-NOESY centered over aromatic ^{13}C.
[i] ^{13}C-edited/^{13}C-filtered 2D NOESY to observe heme-to-protein NOEs.
[j] ^{13}C-filtered/^{13}C-filtered 2D NOESY to observe heme-to-heme NOEs.

viously described methods; Cross and Wright, 1985) from a model structure (Alam et al., 1994b) of this protein were subtracted from all $^{1}H^{\alpha}$ shifts prior to CSI calculation. No compensation of this type was performed for the ^{13}C chemical shifts. A CSI consensus (with and without ring current corrections) was derived from the four individual CSI values using the following criteria: for non-glycine residues, at least three of the four individual CSI values for each residue had to agree as to secondary structure type; for glycines two of the three CSI values had to agree. The consensus CSI were set to 0 when these criteria were not met. Helix initiation and termination points were determined from the consensus CSI (Wishart et al., 1992; Wishart and Sykes, 1994) and the combination of NOE patterns and $^{3}J_{HNH\alpha}$ values. Possible helix-capping interactions (Presta and Rose, 1988; Aurora et al., 1994) were identified from $^{13}C^{\alpha}$ and $^{13}C^{\beta}$ CSI values (Gronenborn and Clore, 1994) and NOEs (Zhou et al., 1994).

Results and discussion

Overview

Extensive NMR investigations have been conducted on the monomeric hemoglobins of *Glycera dibranchiata.* Various studies have focused on different oxidation and ligation states of the heme-Fe including the

unligated ferric (Kandler et al., 1984; Constantinidis et al., 1988; Constantinidis and Satterlee, 1993), the ferric-CN forms (Mintorovitch et al., 1990; Alam and Satterlee, 1994, 1995), and the ferrous-CO form studied in this paper (Cooke and Wright, 1985a,b, 1987; Cooke et al., 1987). The ferrous-CO state of GMH4 (GMH4CO) was chosen because it is a physiologically relevant form that is diamagnetic. The NMR spectra of GMH4CO were of high quality and surprisingly well dispersed for a completely helical protein of this size (15642 Da), containing a large number of glycines (20) and alanines (27), sometimes in long uninterrupted stretches. Figure 1 shows a 2D $^{1}H/^{15}N$ SE-HSQC spectrum of GMH4CO with all correlations labeled by residue type and number. The following sections describe (i) assignments of resonances from the backbone, side chain, aromatic, and heme nuclei of GMH4CO; (ii) determination of the secondary structure from analysis of NOE, scalar coupling and chemical shift data; (iii) recalibration of H^{α} CSI values after correction of heme ring current shifts; and (iv) determination of the topology of the heme active site from analysis of heme–protein NOEs.

Resonance assignments

Resonance assignments for the backbone nuclei ($^{1}H^{N}$, ^{15}N, $^{13}C'$, $^{13}C^{\alpha}$, and $^{1}H^{\alpha}$) were made by analysis of the data from the 3D HNCO, HCACO, HNCA, HN(CO)CA, HNCACB, CBCA(CO)NH, ^{15}N-TOCSY-HSQC, and 2D HSQC experiments (summarized in Table 1). The CBCA(CO)NH and HNCACB data were combined to determine interresidue connections (supplementary material Figure 1). Once a stretch of backbone connectivities was completed, amino acid types were identified from a combination of $^{13}C^{\alpha}$, $^{13}C^{\beta}$ and side-chain ^{1}H chemical shifts. Since this protein is highly helical, the H^{α}-H^{N} TOCSY transfer is inefficient due to the small $^{3}J_{HNH\alpha}$ coupling constants, making complete spin-system identification by this means alone very difficult. However, spin systems for the 27 Ala, 20 Gly, 2 Thr, 11 Val and 12 Ser residues were easily identified in the above manner.

Figure 2 summarizes the backbone assignment data in the rows labeled HNCO and HNCαCβ. The backbone assignments were confirmed by reference to sequential NOEs in the ^{15}N-edited NOESY data set (Figure 2), and are complete except for the $^{1}H^{N}$, ^{15}N and $^{13}C'$ of Gly^{1}. The C(CO)NH-TOCSY experiment provided assignments for aliphatic ^{13}C resonances (Figure 2 C(CO)NH row). From the nearly complete set of ^{13}C side-chain assignments and partially complete ^{1}H side-chain assignments (^{15}N-TOCSY/NOESY), the remaining aliphatic side-chain ^{1}H resonance assignments were obtained from the HCCH-TOCSY and the ^{15}N- and ^{13}C-edited 3D NOESY. Overall, the aliphatic side-chain assignments were comprehensive, with the exception of Lys^{91} H^{γ} and Lys^{96} H^{δ}, H^{γ} protons due to intraresidue degeneracy.

Aromatic side-chain assignments were achieved using 2D $^{1}H/^{1}H$ TOCSY and NOESY experiments on unlabeled protein, as well as ^{13}C-edited TOCSY and NOESY experiments on the $^{13}C/^{15}N$-labeled protein. The spin systems of all phenylalanines (except for Phe^{34}) and both tryptophans were completely assigned, but only tentative assignments were reached for Tyr^{102} and Tyr^{134}. No signals were detected for Tyr^{93}. Because Tyr^{93} lies close to the heme where ring current shifts differing by up to 3 ppm for the two sides of the ring were calculated for both the $H^{\delta 1/\delta 2}$ and $H^{\epsilon 1/\epsilon 2}$, ring flipping in an intermediate exchange regime would account for the lack of signals. The histidine spin systems were assigned, including the $N^{\delta 1}$ and $N^{\epsilon 2}$ nitrogen resonances, using an HMBC experiment (Pelton et al., 1993).

Specific assignment of prochiral resonances quickly improves the precision of NOE-derived distance constraints. Figure 3 contains strips from the HN(CO)HB and HNHB experiments for a region of GMH4CO. The occurrence of strong and weak (or missing) peaks for each H^{β} proton in each strip was used in combination with data from the 3D ^{15}N-edited NOESY-HSQC and TOCSY-HSQC experiments to specifically assign $H^{\beta 2}$ and $H^{\beta 3}$ resonances and make a qualitative determination of χ^{1} (Powers et al., 1993). Of the 81 residues of GMH4CO that contain β-methylene pairs, 43 were assigned stereospecifically; of the 38 remaining residues, 21 had degenerate chemical shifts and 17 showed evidence for rotamer averaging.

An analogous method was used to determine χ^{1} torsion angles for Val, Ile, and Thr residues, as well as to obtain stereospecific assignments for the γ-methyls of all valines in GMH4CO ($\chi^{1} = 180^{\circ}$ in all cases). χ^{1} angles were obtained for all Thr and Ile residues, except for Ile^{118}, which appeared to be undergoing rotational averaging. The H^{δ} methyl signals from six of the 10 Leu residues were assigned stereospecifically by combining intraresidue NOE information, with stereoassignments of the H^{β} protons and long-range carbon–carbon coupling constants (Powers et al., 1990; Bax et al., 1992).

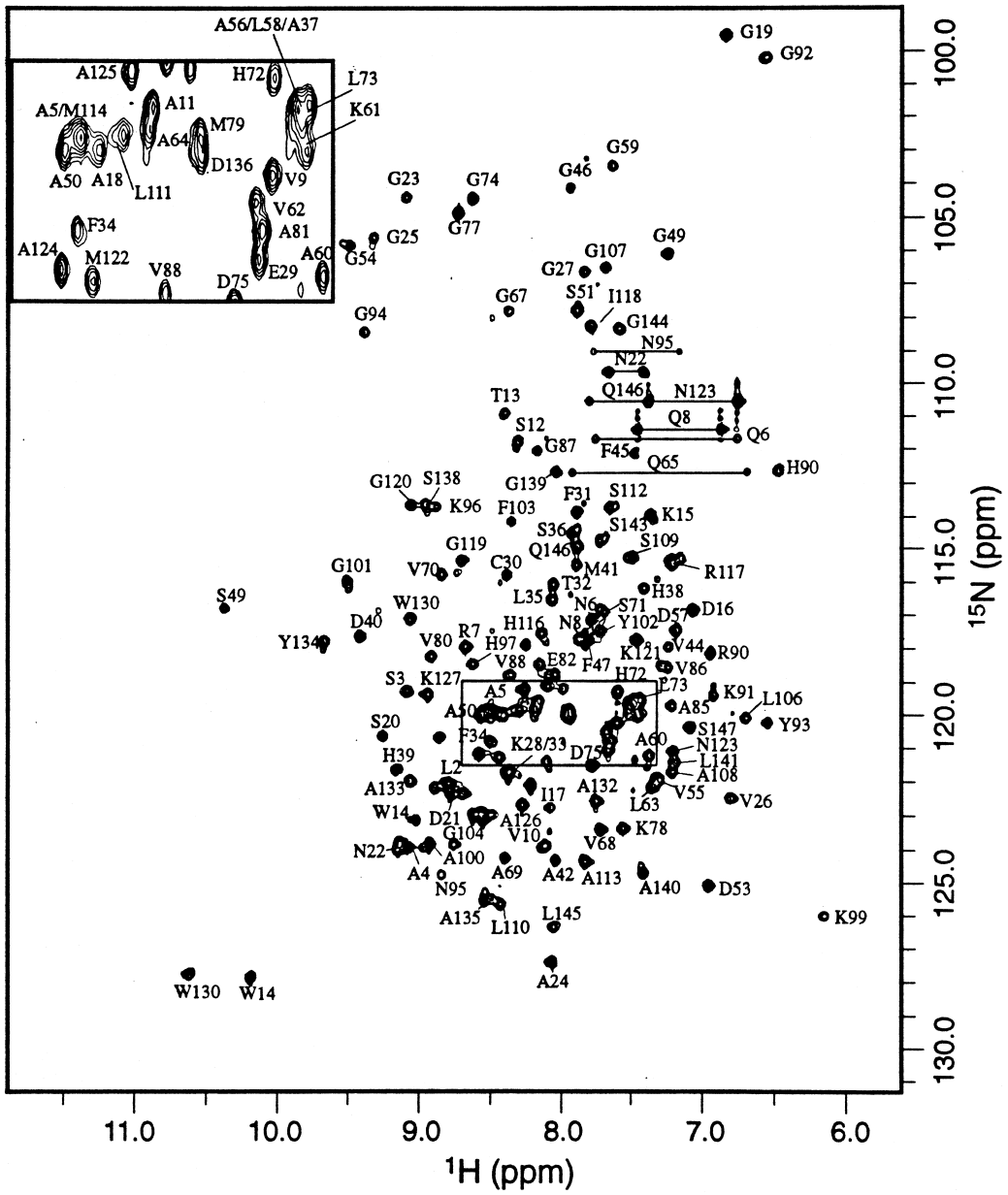

Figure 1. Gradient-enhanced $^{1}H/^{15}N$ HSQC of [$^{15}N/^{13}C$]-GMH4CO (3 mM) in 90% H_2O at pH 5.0 and 293 K. All amide $^{1}H/^{15}N$ correlations are labeled according to their primary sequence position. The side-chain amide resonances for the glutamine and asparagine side chains are connected by horizontal lines and labeled. Signals from exchangeable indole protons ($H^{\epsilon 1}$) of the two tryptophans (Trp^{14}, Trp^{130}) are also labeled. The inset details a region of high degeneracy.

The heme-b prosthetic group of this protein is buried within the protein interior. In preparation for a detailed structure determination, unambiguous assignments of this group were pursued, since a large number of crucial long-range NOE restraints were expected to involve the heme. Most of the heme assignments presented here confirm earlier assignments made for the CO-ligated form of this protein (Cooke and Wright, 1985a,b, 1987; Cooke et al., 1987). This work expands on those heme assignments by including the two propionic acid side chains. Since the $^{13}C/^{15}N$-labeled protein was reconstituted with b-type heme at natural abundance, ^{13}C filtering methods could be used in assigning the heme resonances. Figure 4B

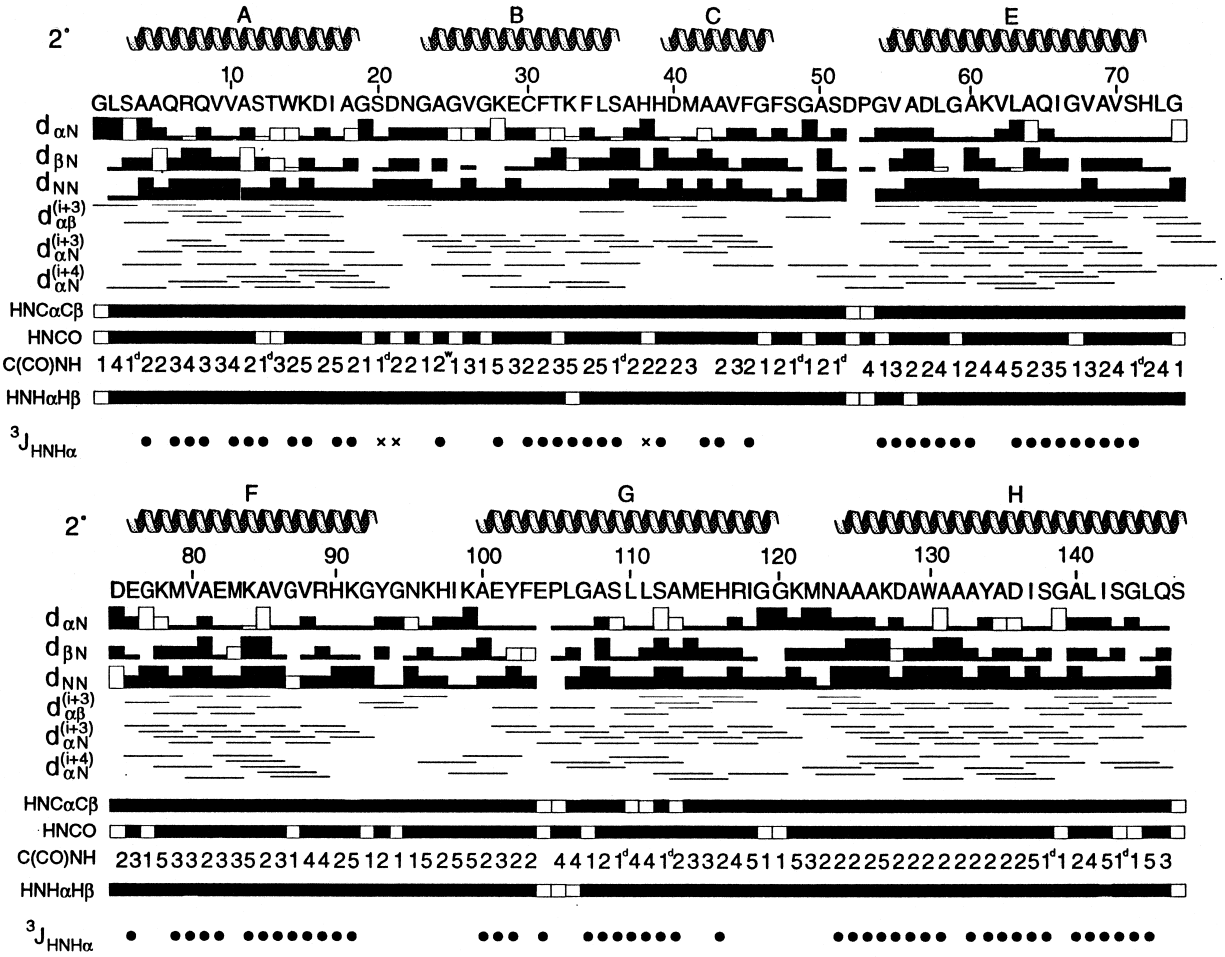

Figure 2. Summary of sequential NOEs ($d_{\alpha N}$, $d_{\beta N}$, d_{NN}), medium-range NOEs ($d_{\alpha\beta}^{i+3}$, $d_{\alpha N}^{i+3}$, $d_{\alpha N}^{i+4}$), backbone assignment information (HN-CACB, HNCO, C(CO)NH, HNHAHB), and $^3J_{HNH\alpha}$ scalar coupling information. The intensity of each sequential NOE (strong, medium, weak) is represented by the height of the box at that position. Filled boxes represent fully resolved NOEs; empty boxes represent overlapped NOEs with greater uncertainty in NOE intensity. Detected medium-range NOEs are represented by a horizontal line connecting the residues involved. Filled boxes in the HNCACB row represent cases where data from the HNCA, HNCACB, CBCA(CO)NH, and HN(CO)CA experiments all agreed on assignments for intervening $^1H^N/^{13}C^\alpha/^{13}C^\beta$ building blocks. Filled boxes in the HNCO row denote cases where the HNCO and HCACO experiments yielded a common intervening carbonyl resonance. Numbers in the C(CO)NH row correspond to the sum of aliphatic carbons, for each side chain, as observed in the C(CO)NH-TOCSY experiment. The HNHAHB row has filled boxes where the ^{15}N-edited TOCSY-HSQC and the HBHA(CBCACO)NH experiments agree on intervening $^1H^\alpha$ and $^1H^\beta$ shifts. Empty boxes denote where assignments are supported by data from only one of the experiments. The $^3J_{HNH\alpha}$ row indicates qualitatively the value of this J-coupling constant as either less than 5 Hz (•), typical of helical regions, or greater than 8 Hz (×); no designation indicates an intermediate or undetermined value. Positions of α-helices (A–H) as determined by analysis of NOE and $^3J_{HNH\alpha}$ patterns are indicated above the amino acid sequence and labeled as in the model structure of GMH4 (Alam et al., 1994b).

shows the complete $^{13}C/^{13}C$-filtered 2D NOESY spectrum for the $^{13}C/^{15}N$-labeled GMH4CO sample in 90% H_2O. Only cross peaks involving ^{12}C-attached protons as the source and destination of the NOE were observed (i.e., only heme–heme NOEs). Starting at the HD meso, NOEs can be traced through the C-vinyl group to the C-methyl, to the C-meso and the B-vinyl, to the B-methyl, and the B-meso. Progressing from the B-meso, NOEs were observed to the A-methyl group, next to the A-propionate, then to the A-meso, to the D-propionate, to the D-methyl, and finally back to the D-meso. None of these sequential assignments required intervening protein contacts, much like the spectral analysis of the paramagnetic CN^- form (Alam and Satterlee, 1994, 1995). Assignments for the two propionic acid side chains are reported in this

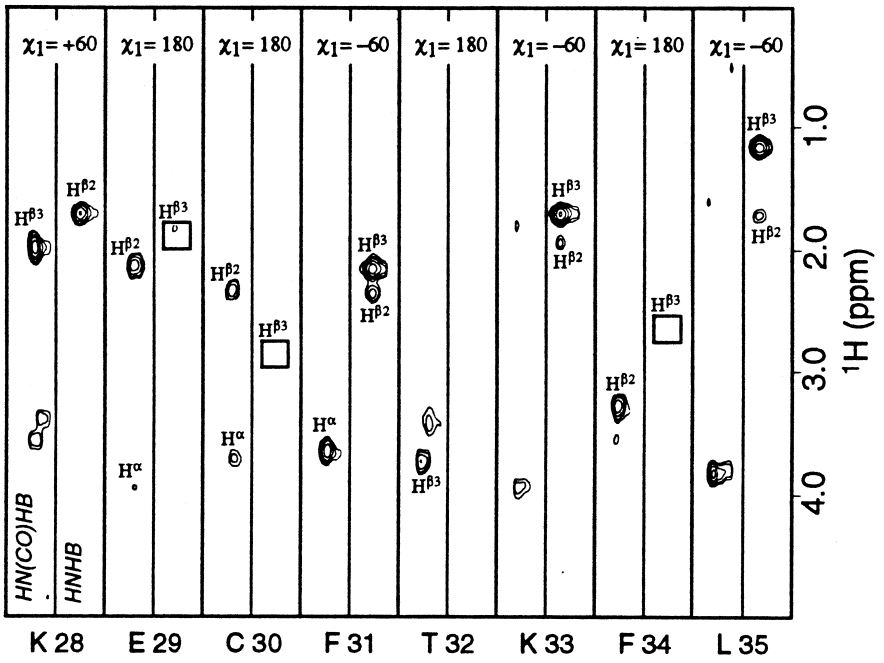

Figure 3. An alternating HN(CO)HB and HNHB strip plot for residues Lys[28] to Leu[35]. The H^{α} and H^{β} resonances in each strip are labeled. These data were used to determine stereospecific assignments for the β-methylenes and to obtain χ^1 angle information (Powers et al., 1993). The χ^1 torsion angle defined for each residue is given above each strip pair.

ligation state for the first time. The NOEs in Figure 4B from the two vinyl groups to the neighboring heme substituents placed the vinyl groups in a rotomer orientation roughly similar to that depicted in Figures 4A and 6B.

Secondary structure

Identification of secondary structural elements in proteins has traditionally relied upon patterns of NOEs (Wüthrich, 1986) and, more recently, ^{1}H and ^{13}C chemical shifts (Robertson et al., 1990; Spera and Bax, 1991; Wishart et al., 1992, 1995a; Wishart and Sykes, 1994). Figure 2 summarizes the strong d_{NN} and $d_{\beta N}$ sequential NOEs and medium-range NOE types observed for α-helices. Figure 2 also includes the $^3J_{HNH\alpha}$ values determined with the HNHA experiment. Small $^3J_{HNH\alpha}$ couplings (•) are typical of helical regions while larger scalar couplings (×) are indicative of β-sheet or turn. From this information seven helical stretches were defined (residues 3–19, 23–36, 39–46, 54–72, 76–92, 101–119, 124–146), connected by six turn regions (residues 20–22, 37–38, 47–53, 73–75, 93–100, 120–123).

Figure 5 shows the chemical shift deviations from random coil values (CSI) for each assigned $^{13}C'$, $^{13}C^{\alpha}$, $^{13}C^{\beta}$, and $^1H^{\alpha}$ resonance, as well as the consensus CSI for each residue. The consensus CSI term also defines seven helical regions (4–19, 24–36, 39–42, 53–71, 76–91, 100–121, 124–144). In addition, $^{13}C^{\alpha}$ and $^{13}C^{\beta}$ secondary shifts characteristic of helix-capping interactions (Gronenborn and Clore, 1994) are observed for residues Ser[3], Asp[52], Asp[75], and Lys[99]. Except for Lys[99], these residues have the potential to form side-chain/main-chain hydrogen bonds to stabilize the helix N-terminus (Presta and Rose, 1988; Zhou et al., 1994). Evidence that the sequence S^3AAQ^6 forms the two reciprocal hydrogen bonds characteristic of a capping box is provided by characteristic NOEs from Ser^3 H^N to Gln^6 $H^{\beta 3}$ and Ser^3 $H^{\beta 2}$ to Ala^5 H^N. Five of the helices (A, C, F, G, and H) may be involved in C-terminal helix-capping motifs involving glycine (Aurora et al., 1994), but without a knowledge of hydrogen bonding patterns (i.e., from NH exchange) a precise description is not possible.

Heme ring current shifts

In contrast to the helix designations derived from NOE and $^3J_{HNH\alpha}$ data, helix C ends four residues early in the uncorrected consensus CSI analysis (Figure 5; CSI blank bars). In addition, gaps are observed in the CSI for helices A, E, G and H. To test whether this lack of agreement lies in the fact that the CSI is an empir-

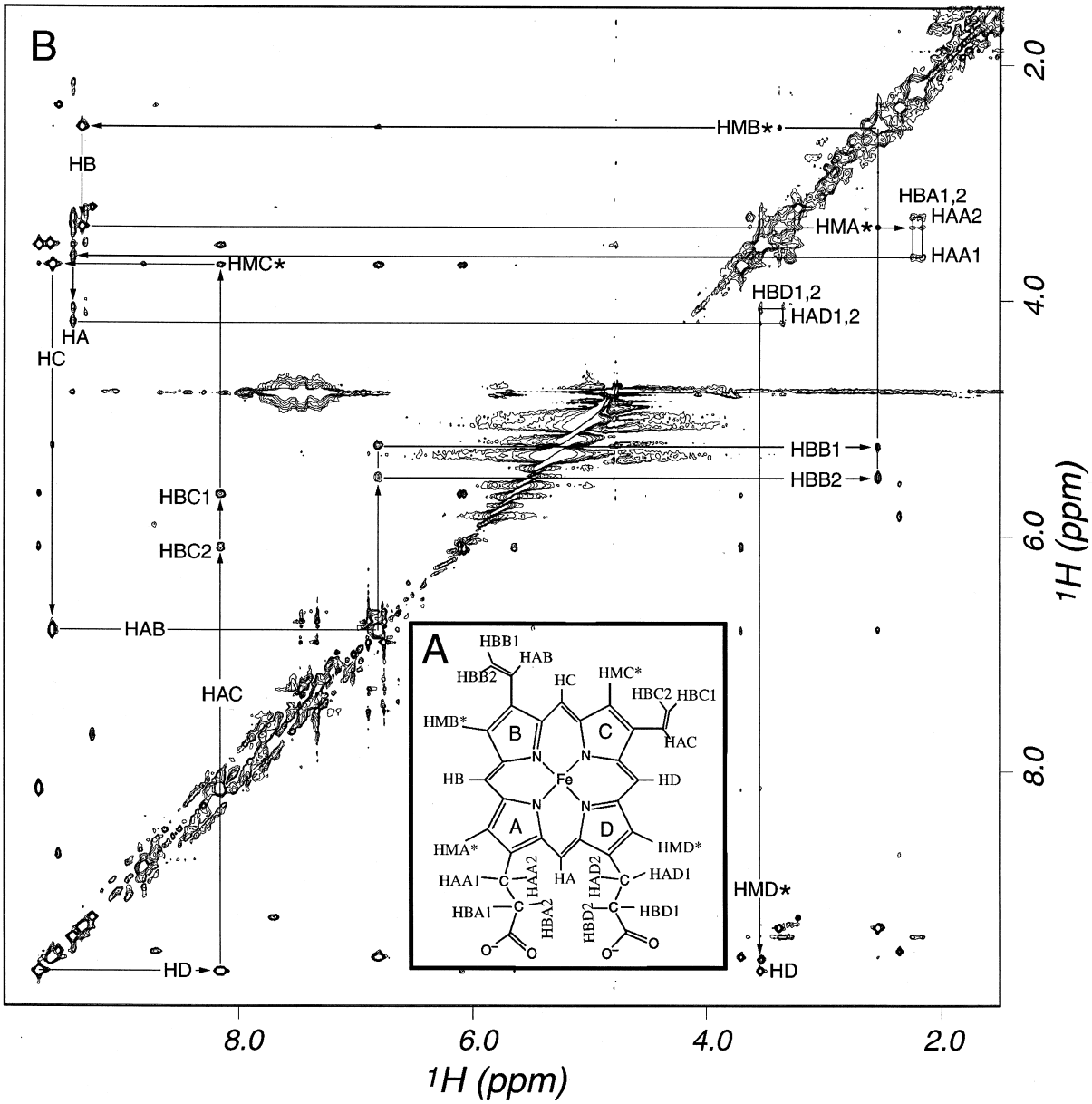

Figure 4. Atom nomenclature and NMR assignments for the heme-b prosthetic group in GMH4CO. (A) Heme-b structure with all proton positions labeled according to the X-PLOR nomenclature (CHARMM22). Orientation is depicted as though looking from the distal side toward the heme in GMH4CO (Alam et al., 1994b). Methyl group protons are labeled as pseudoatoms (i.e., HMB1,2,3 = HMB*). (B) The entire $^{13}C/^{13}C$-filtered 2D ^{1}H-NOESY (125 ms mixing time) for the [$^{15}N/^{13}C$]-GMH4CO sample in 90% H_2O and at 293 K, which shows only the heme–heme NOE interactions. Sequential ^{1}H NOEs are connected by arrows in a manner that allows consecutive NOE connections to be traced around heme-b in a counterclockwise fashion starting at the HD meso proton (lower left).

ically defined index of chemical shifts that does not take into account the considerable ring current shifts induced by the heme prosthetic group on nearby spins, a simple ring current shift calculation based on the model structure (Alam et al., 1994b) was performed for all assigned $^{1}H^{\alpha}$ protons (Figure 5; RCS). Ring current contributions to the observed $^{1}H^{\alpha}$ shifts were calculated by methods previously described (Cross and Wright, 1985) and subtracted from each observed shift ($^{1}H^{\alpha}$-RCS). Adjustment to only one component of the CSI index resulted in improved secondary structure definition for certain regions, as indicated by gray

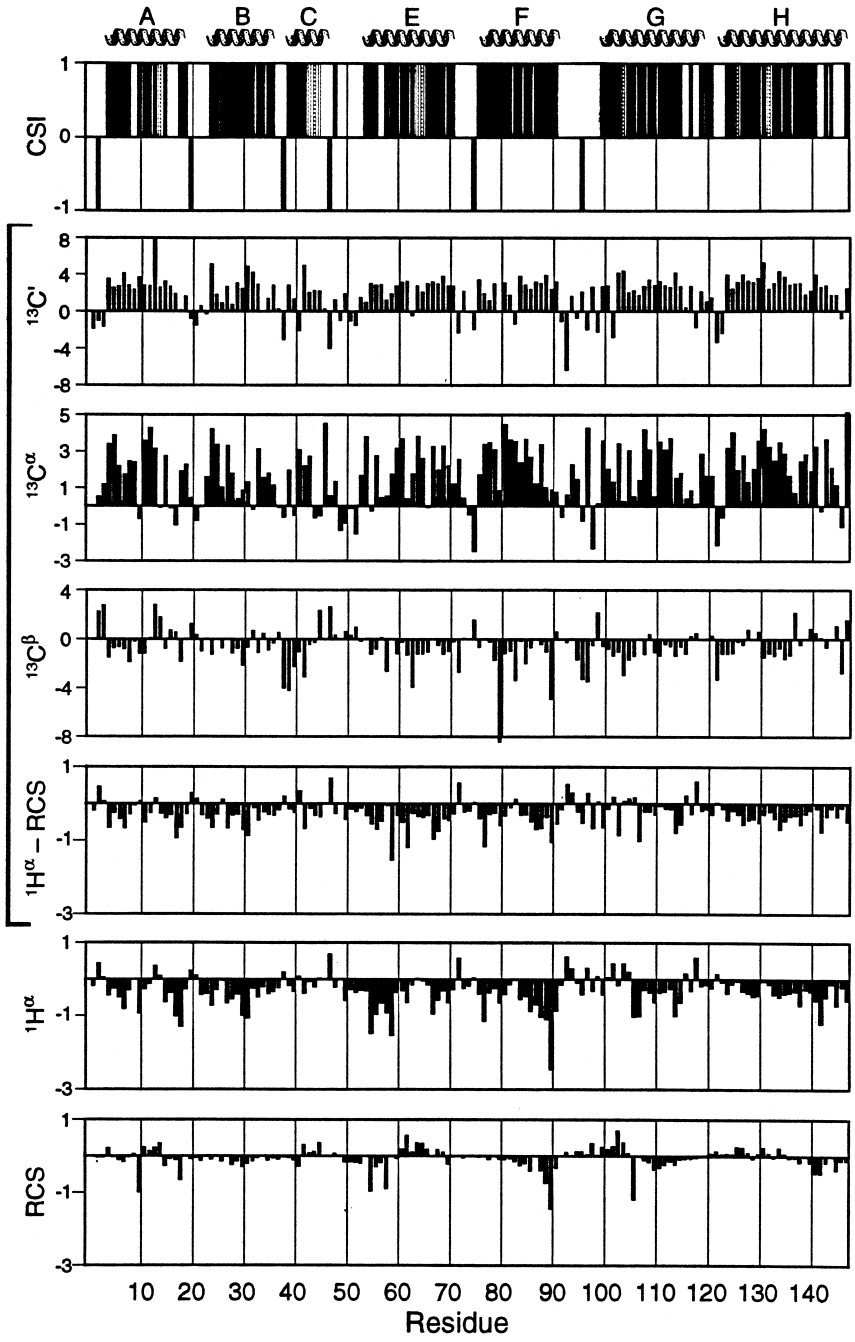

Figure 5. CSI values for GMH4CO. Seven separate plots are shown, including a consensus CSI, secondary shifts for $^{13}C'$, $^{13}C^{\alpha}$, $^{13}C^{\beta}$, and $^{1}H^{\alpha}$ resonances of each residue, calculated ring current contributions to $^{1}H^{\alpha}$ shifts (RCS), and the $^{1}H\alpha$ CSI corrected for the ring current shift contributions to the observed shift ($^{1}H^{\alpha}$-RCS). The consensus CSI was determined from the CSI values for the four individual shifts. The bracket indicates the four individual CSI values used to define a consensus CSI. A positive consensus CSI was assigned when at least three of the four individual CSI terms suggested a helical region. A negative CSI was assigned when three of four of the CSI values suggested β-sheet, while a zero CSI was given when there was no agreement within the four CSI values. For glycine residues, only two of three CSI values ($^{13}C'$, $^{13}C^{\alpha}$, and mean $^{1}H^{\alpha}$) had to agree to assign a consensus value. Gray bars in the consensus CSI indicate residues at which the correction of the α-proton chemical shift, by subtracting the calculated contributions of ring currents from the $^{1}H^{\alpha}$ observed shifts, led to positive CSI values. Helical regions derived from NOE data (Figure 2), indicated above the consensus, provide a comparison of the two secondary structure determination methods.

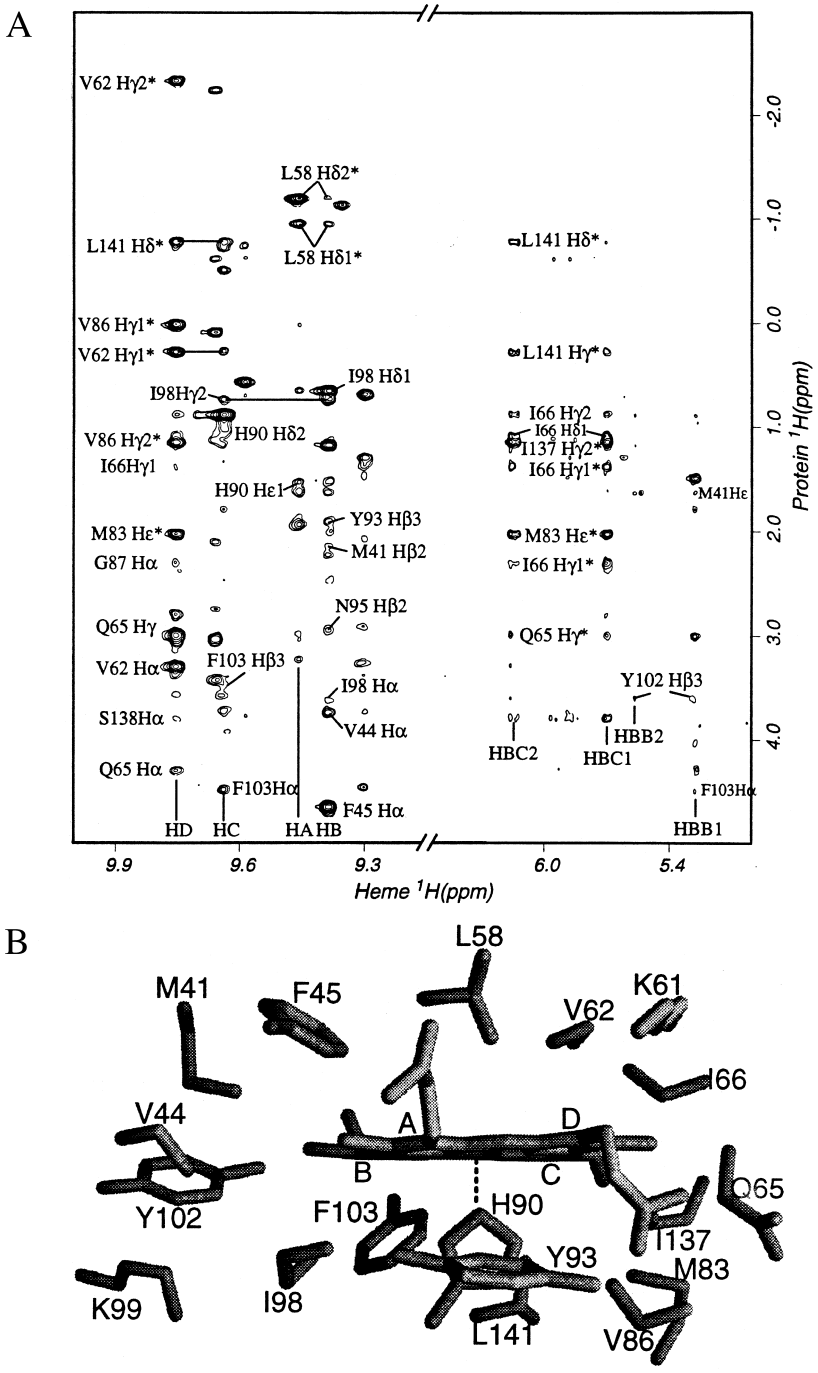

Figure 6. Heme pocket topology. (A) Expansions of the ^{13}C-filtered/^{13}C-edited 2D NOESY (120 ms mixing time) of the [^{13}C/^{15}N]-labeled GMH4CO in 90% H_2O. These expansions show heme–protein ^{1}H/^{1}H NOEs for all four heme meso protons and the four β-vinyl protons. These interactions are labeled by the amino acid/heme constituents involved (D2 and D1, respectively) using X-PLOR nomenclature for the heme group (Figure 4A). For both sets of β-vinyl protons, NOEs experienced by both protons are only labeled once. This expansion represents only a small subset of the 130 heme–protein NOEs observed. (B) The heme environment including all amino acids involved in heme–protein NOEs labeled at their unrefined positions relative to the heme. The diagram was constructed using GRASP (Nicholls et al., 1991) and the coordinates of the model structure of deoxy-GMH4 (Alam et al., 1994b). Only residues that exhibited heme-protein NOEs (i.e., data from the 2D ^{13}C-edited/^{13}C-filtered NOESY, the 3D ^{13}C-NOESY-HSQC, or the 3D ^{15}N-NOESY-HSQC experiments) are included in the figure.

bars in the consensus CSI (Figure 5). Most significant was the change in the extent of the C helix, which was defined to include residues 39–42 prior to RCS recalibration of the consensus CSI, but was extended to residue 45 after adjustment (Figure 5; $^{1}H^{\alpha}$-RCS and consensus CSI gray bars). This result agrees with the definition of the C helix by additional NMR data discussed above.

Heme pocket description

With complete resonance assignments, positioning of the heme within the protein matrix was accomplished with NOE information. A similar approach to that described for the heme assignments was used to identify heme–protein specific NOEs. Figure 6A shows two expansions of a ^{13}C-edited/^{13}C-filtered 2D NOESY with assignments labeled specifically for the heme meso protons (HA–HD; Figure 4A) and heme vinyl substituents (see Figure 4A for labels). The heme proton involved in the NOE is identified along the horizontal axis while the protein resonance is labeled vertically within the figure. A total of 130 heme–protein NOEs were identified in this manner and further confirmed in the 3D ^{13}C- and ^{15}N-edited NOESY data. This set of NOE-defined interactions was used to qualitatively assess the heme site of the earlier proposed model. Figure 6B depicts the heme ligand binding site which includes all the protein side chains about the heme that have heme contacts. Also labeled about the heme are the heme pyrroles (A–D). The NMR data support the model proposed previously for the active site in that 18 residues (Met^{41}, Val^{44}, Phe^{45}, Leu^{58}, Lys^{61}, Val^{62}, Gln^{65}, Ile^{66}, Met^{83}, Val^{86}, His^{90}, Tyr^{93}, Ile^{98}, Lys^{99}, Tyr^{102}, Phe^{103}, Ile^{137}, and Leu^{141}) are placed in close contact with the heme. The heme–protein NOEs alone suffice to position the heme with respect to each of the amino acid side chains. Although the data are so extensive that they cannot all be shown in Figure 6A, the results indicate that near the A-pyrrole (HMA* and HAA*, HBA*; see Figure 4A) are amino acids Ile^{98}, Val^{44}, Lys^{99}, Phe^{45}, Leu^{58}, and Tyr^{93}. Close to the B-pyrrole are Tyr^{102}, Val^{44}, Phe^{103}, and Ile^{98}. In proximity to the C-pyrrole are the side chains of Ile^{66}, Ile^{137}, Gln^{65}, Val^{62}, and Met^{83}. Finally, Leu^{58}, Lys^{61}, Val^{86}, Leu^{141}, and Val^{62} are adjacent to the D-pyrrole. His^{90} is the heme-Fe proximal ligand.

The placement of the side chains above or below the heme required additional information supplied as protein–protein NOEs. These data, obtained from ^{13}C- and ^{15}N-edited NOESY experiments, are consistent with the proposed model structure and earlier NMR work that described the active site of this protein (monomeric protein A (Cooke and Wright, 1985a; Cooke et al., 1987)). Of particular interest was the placement of Phe^{31}(B10), which was located above the heme in the model structure. Phe^{31}was placed above the heme iron on the basis of interresidue NOEs between Phe^{31} and Phe^{45}, Leu^{58}, Val^{62}, Leu^{63}, and Leu^{106} observed in the ^{13}C-edited 3D NOESY data. NOEs between Phe^{31} and the peripheral heme substituents, however, were not visible in the edited spectra probably because of its distance from the heme (>5 Å). For this reason Phe^{31} was omitted from Figure 6B.

Conclusions

The present results provide a qualitative description of the secondary structure of this protein in solution. The global secondary structure elements defined by this work agree in all respects with a structure predicted by molecular modeling (Alam et al., 1994b) which in turn was based on the crystal structure of a related hemoglobin (Arents and Love, 1989). The results illustrate the need for cautious use of the CSI for secondary structure determination in proteins containing conjugated prosthetic groups or other ligands that produce appreciable diamagnetic anisotropy. Heme–protein contacts developed from selectively observed heme NOEs have been used to verify the placement of the heme in its binding pocket. The results confirm the unusual occurrence of both Phe^{31}(B10) and Leu^{58}(E7) in the distal ligand binding pocket. These two amino acids are uniquely situated to influence ligand binding, heme orientation, and to contribute to the non-polar heme environment that must be the structural basis for the anomalous ligand binding kinetics that are the functional hallmark of component IV of *Glycera dibranchiata* monomeric hemoglobin. This completes the ^{1}H, ^{13}C, and ^{15}N resonance assignments for GMH4CO, including all ^{1}H assignments of the heme prosthetic group. These data have been deposited in the BioMagResBank (http://www.bmrb.wisc.edu) at the University of Wisconsin-Madison (BMRB accession #4038).

Acknowledgements

The authors thank Dr. Steve Sukits for performing the ring current calculations on GMH4CO, Dr. Gerd La

Mar of the University of California, Davis, for supplying the program for this calculation, and Dr. Chad C. Nelson of the University of Utah for mass spectrometry analysis of the protein. They also thank Dr. Ed Mooberry and other members of the staff at NMRFAM for their gracious help. This work was supported by the National Institutes of Health (GM47645, J.D.S.; GM35976, J.L.M.). Equipment in NMRFAM was purchased with funds from the University of Wisconsin, the NSF Biological Instrumentation Program (Grant DMB-8415048), the NIH Biomedical Research Technology Program (Grant RR02301), the NIH Shared Instrumentation Program (Grant RR02781), and the U.S. Department of Agriculture. Support for the NMR instrumentation at WSU came from NIH (RR06312011) and from the Battelle Pacific Northwest National Laboratory.

References

Adachi, S., Sunohara, N., Ishomori, K. and Morishima, I. (1992) *J. Biol. Chem.*, **267**, 12614–12621.

Alam, S.L., Dutton, D.P. and Satterlee, J.D. (1994a) *Biochemistry*, **33**, 10337–10344.

Alam, S.L., Satterlee, J.D. and Edmonds, C.G. (1994b) *J. Protein Chem.*, **13**, 151–164.

Alam, S.L. and Satterlee, J.D. (1994) *Biochemistry*, **33**, 4008–4018.

Alam, S.L. and Satterlee, J.D. (1995) *J. Am. Chem. Soc.*, **117**, 49–53.

Archer, S.J., Ikura, M., Torchia, D.A. and Bax, A. (1991) *J. Magn. Reson.*, **95**, 636–641.

Arents, G. and Love, W.E. (1989) *J. Mol. Biol.*, **210**, 149–161.

Aurora, R., Srinivasan, R. and Rose, G.D. (1994) *Science*, **264**, 1126–1129.

Baldwin, J. and Chothia, C. (1979) *J. Mol. Biol.*, **129**, 175–220.

Bax, A., Max, D. and Zax, D. (1992) *J. Am. Chem. Soc.*, **114**, 6923–6925.

Bazzo, R., Cicero, D.O. and Barbato, G. (1995) *J. Magn. Reson.*, **B107**, 189–191.

Braden, B.C., Arents, G., Padlan, E.A. and Love, W. E. (1994) *J. Mol. Biol.*, **238**, 42–53.

Carver, T.E., Olson, J.S., Smerdon, S.J., Krzywda, S., Wilkinson, A.J., Gibson, Q.H., Blackmore, R.S., Ropp, J.D. and Sligar, S.G. (1991) *Biochemistry*, **30**, 4697–4705.

Carver, T.E., Brantley, R.E., Singleton, E.W., Arduini, R.M., Quillin, M.L., Phillips, G.N. and Olson, J.S. (1992) *J. Biol. Chem.*, **267**, 14443–14450.

Case, D.A. and Karplus, M. (1979) *J. Mol. Biol.*, **132**, 343–368.

Constantinidis, I., Satterlee, J.D., Pandey, R.K., Leung, H. and Smith, K.M. (1988) *Biochemistry*, **27**, 3069–3076.

Constantinidis, I. and Satterlee, J.D. (1993) *Biophys. (Life Sci. Adv.)*, **12**, 99–107.

Cooke, R.M. and Wright, P.E. (1985a) *Biochim. Biophys. Acta*, **832**, 357–364.

Cooke, R.M. and Wright, P.E. (1985b) *Biochim. Biophys. Acta*, **832**, 365–372.

Cooke, R.M., Dalvit, C., Narula, S.S. and Wright, P.E. (1987) *Eur. J. Biochem.*, **166**, 399–408.

Cooke, R.M. and Wright, P.E. (1987) *Eur. J. Biochem.*, **166**, 409–414.

Cross, K.J. and Wright, P.E. (1985) *J. Magn. Reson.*, **64**, 220–231.

Edison, A.S., Abildgaard, F., Westler, W.M., Mooberry, E.S. and Markley, J.L. (1994) *Methods Enzymol.*, **239**, 3–79.

Egeberg, K.D., Springer, B.A., Sligar, S.G., Carver, T.E., Rohlfs, R.J. and Olson, J.S. (1990) *J. Biol. Chem.*, **265**, 11788–11795.

Gibson, Q.H., Regan, R., Elber, R., Olson, J.S. and Carver, T.E. (1992) *J. Biol. Chem.*, **267**, 22022–22034.

Green, B.N., Sannes-Lowery, K.A., Loo, J.A., Satterlee, J.D., Kuchumov, A.R., Walz, D.A. and Vinogradov, S.N. (1997) *J. Protein Chem.*, **17**, 85–97.

Gronenborn, A.M. and Clore, G.M. (1994) *J. Biomol. NMR*, **4**, 455–448.

Grzesiek, S. and Bax, A. (1992) *J. Magn. Reson.*, **96**, 432–440.

Grzesiek, S., Ikura, M., Clore, G.M., Gronenborn, A.M. and Bax, A. (1992) *J. Magn. Reson.*, **96**, 215–221.

Grzesiek, S., Anglister, J. and Bax, A. (1993a) *J. Magn. Reson.*, **B101**, 114–119.

Grzesiek, S., Vuister, G.W. and Bax, A. (1993b) *J. Biomol. NMR*, **3**, 487–493.

Grzesiek, S. and Bax, A. (1993) *J. Biomol. NMR*, **3**, 185–204.

Ideka-Saito, M., Lutz, R.S., Shelley, D.A., McKelvey, E.J., Mattera, R. and Hori, H. (1991) *J. Biol. Chem.*, **266**, 23641–23647.

Ikura, M. and Bax, A. (1992) *J. Am. Chem. Soc.*, **114**, 2433–2440.

Kandler, R.L. and Satterlee, J.D. (1983) *Comp. Biochem. Physiol.*, **75B**, 499–503.

Kandler, R.L., Constantinidis, I. and Satterlee, J.D. (1984) *Biochem. J.*, **226**, 131–138.

Kay, L.E., Ikura, M., Tschudin, R. and Bax, A. (1990) *J. Magn. Reson.*, **89**, 496–514.

Kay, L.E., Xu, G.-Y., Singer, A.U., Muhandiram, D.R. and Forman-Kay, J.D. (1993) *J. Magn. Reson.*, **B101**, 333–337.

Kay, L.E., Xu, G.Y. and Yamazaki, T. (1994) *J. Magn. Reson.*, **A109**, 129–133.

Kottalam, J. and Case, D.A. (1988) *J. Am. Chem. Soc.*, **110**, 7690–7697.

Kuboniwa, H., Grzesiek, S., Delaglio, F. and Bax, A. (1994) *J. Biomol. NMR*, **4**, 871–878.

Lambright, D.G., Balesubramanian, S. and Boxer, S.G. (1989) *J. Mol. Biol.*, **207**, 289–299.

Lee, W., Revington, M.J., Arrowsmith, C. and Kay, L.E. (1994) *FEBS Lett.*, **350**, 87–90.

Maniatis, T., Fritsch, E.F. and Sambrook, J. (1986) *Molecular Cloning: A Laboratory Manual*, Cold Spring Harbor Laboratory, Cold Spring Harbor, NY.

Marion, D. and Wüthrich, K. (1983) *Biochem. Biophys. Res. Commun.*, **113**, 967–974.

McCoy, M.A. and Mueller, L. (1992) *J. Am. Chem. Soc.*, **114**, 2108–2112.

Mintorovitch, J. and Satterlee, J.D. (1988) *Biochemistry*, **27**, 8045–8050.

Mintorovitch, J., van Pelt, D. and Satterlee, J.D. (1989) *Biochemistry*, **28**, 6099–6104.

Mintorovitch, J., Satterlee, J.D., Pandey, R.K., Leung, H. and Smith, K.M. (1990) *Inorg. Chim. Acta*, **170**, 157–159.

Muhandiram, D.R. and Kay, L.E. (1994) *J. Magn. Reson.*, **B103**, 203–216.

Nicholls, A., Sharp, K. and Honig, B. (1991) *Proteins Struct. Funct. Genet.*, **11**, 281–296.

Olson, J.S., Mathews, A.J., Rohlfs, R.J., Springer, B.A., Egeberg, K.D., Sligar, S.G., Tame, J., Renaud, J.-P. and Nagai, K. (1988) *Nature*, **336**, 265–266.

Padlan, E.A. and Love, W.E. (1968) *Nature*, **220**, 376–378.

Parkhurst, L.J., Sima, P. and Goss, D.J. (1980) *Biochemistry*, **19**, 2688–2692.
Pelton, J.G., Torchia, D.A., Meadow, N.D. and Roseman, S. (1993) *Protein Sci.*, **2**, 543–558.
Perutz, M.F., Fermi, G., Luisi, B., Shaanan, B. and Liddington, R.C. (1987) *Acc. Chem. Res.*, **20**, 309–321.
Petric, J.W., Lambry, J., Kuczera, K., Karplus, M., Poyart, C. and Martin, J. (1991) *Biochemistry*, **30**, 3975–3987.
Piotto, M., Saudek, V. and Sklenar, V. (1992) *J. Biomol. NMR*, **2**, 661–665.
Powers, R., Garrett, D.S., March, C.J., Frieden, E.A., Gronenborn, A.M. and Clore, G.M. (1993) *Biochemistry*, **32**, 6744–6762.
Presta, L.G. and Rose, G.D. (1988) *Science*, **240**, 1632–1641.
Quillin, M.L., Arduini, R.M., Olson, J.S. and Phillips, G.N. (1993) *J. Mol. Biol.*, **234**, 140–155.
Robertson, A.D., Rhyu, G.I., Westler, W.M. and Markley, J.L. (1990) *Biopolymers*, **29**, 461–467.
Rohlfs, R.J., Mathews, A.J., Carver, T.E., Olson, J.S., Springer, B.A., Egeberg, K.D. and Sligar, S.G. (1990) *J. Biol. Chem.*, **265**, 3168–3176.
Santoro, J. and King, G.C. (1992) *J. Magn. Reson.*, **97**, 202–207.
Shaanan, B. (1983) *J. Mol. Biol.*, **171**, 31–59.
Smerdon, S.J., Dodson, G.G., Wilkinson, A.J., Gibson, Q.H., Blackmore, R.S., Carver, T.E., and Olson, J.S. (1991) *Biochemistry*, **30**, 6252–6260.
Spera, S. and Bax, A. (1991) *J. Am. Chem. Soc.*, **113**, 5490–5492.
Srajer, V., Teng, T.-Y., Ursby, T., Pradervand, C., Ren, Z., Adachi, S.-I., Schildkamp, W., Bourgeois, D., Wulf, M. and Moffat, K. (1996) *Science*, **274**, 1726–1729.
Teske, J., Edmonds, C.G., Deckert, G. and Satterlee, J.D. (1997) *J. Protein Chem.*, **16**, 139–150.
Van Zijl, P.C.M., Johnson, M.O., Mori, S. and Hurd, R.E. (1995) *J. Magn. Reson.*, **A113**, 256–270.
Venters, R.A., Calderone, T.L., Spicer, L.D. and Fierke, C.A. (1991) *Biochemistry*, **30**, 4491–4494.
Vuister, G.W. and Bax, A. (1993) *J. Am. Chem. Soc.*, **115**, 7772–7777.
Vuister, G.W., Wang, A.C. and Bax, A. (1993) *J. Am. Chem. Soc.*, **115**, 5334–5335.
Wall, L. and Schwartz, R.L. (1991) *Programming Perl*, O'Reilly and Associates, Sebastopol.
Warren, W.S., Richter, W., Andreotti, A.H. and Farmer II, B.T. (1993) *Science*, **262**, 2005–2009.
Wishart, D.S., Sykes, B.D. and Richards, F.M. (1992) *Biochemistry*, **31**, 1647–1651.
Wishart, D.S. and Sykes, B.D. (1994) *J. Biomol. NMR*, **4**, 171–180.
Wishart, D.S., Bigam, C.G., Holm, A., Hodges, R.S. and Sykes, B.D. (1995a) *J. Biomol. NMR*, **5**, 67–81.
Wishart, D.S., Bigam, C.G., Yao, J., Abildgaard, F., Dyson, H.J., Oldfield, E., Markley, J.L. and Sykes, B.D. (1995b) *J. Biomol. NMR*, **6**, 135–140.
Wittekind, M. and Mueller, L. (1993) *J. Magn. Reson.*, **B101**, 201–205.
Wüthrich, K. (1986) *NMR of Proteins and Nucleic Acids*, Wiley, New York, NY.
Zhang, O., Kay, L.E., Olivier, J.P. and Forman-Kay, J.D. (1994) *J. Biomol. NMR*, **4**, 845–858.
Zhou, H.X., Lyu, P., Wemmer, D.E. and Kallenbach, N.R. (1994) *Proteins Struct. Funct. Genet.*, **18**, 1–7.